Vapor hydrogen and oxygen isotopes reflect water of combustion in the urban atmosphere

Galen Gorski[a], Courtenay Strong[b,c], Stephen P. Good[a], Ryan Bares[c], James R. Ehleringer[c,d], and Gabriel J. Bowen[a,c,1]

[a]Department of Geology & Geophysics, [b]Department of Atmospheric Sciences, [c]Global Change and Sustainability Center, and [d]Department of Biology, University of Utah, Salt Lake City, UT 84112

Edited by Mark H. Thiemens, University of California, San Diego, La Jolla, CA, and approved January 30, 2015 (received for review December 24, 2014)

Anthropogenic modification of the water cycle involves a diversity of processes, many of which have been studied intensively using models and observations. Effective tools for measuring the contribution and fate of combustion-derived water vapor in the atmosphere are lacking, however, and this flux has received relatively little attention. We provide theoretical estimates and a first set of measurements demonstrating that water of combustion is characterized by a distinctive combination of H and O isotope ratios. We show that during periods of relatively low humidity and/or atmospheric stagnation, this isotopic signature can be used to quantify the concentration of water of combustion in the atmospheric boundary layer over Salt Lake City. Combustion-derived vapor concentrations vary between periods of atmospheric stratification and mixing, both on multiday and diurnal timescales, and respond over periods of hours to variations in surface emissions. Our estimates suggest that up to 13% of the boundary layer vapor during the period of study was derived from combustion sources, and both the temporal pattern and magnitude of this contribution were closely reproduced by an independent atmospheric model forced with a fossil fuel emissions data product. Our findings suggest potential for water vapor isotope ratio measurements to be used in conjunction with other tracers to refine the apportionment of urban emissions, and imply that water vapor emissions associated with combustion may be a significant component of the water budget of the urban boundary layer, with potential implications for urban climate, ecohydrology, and photochemistry.

stable isotopes | urban emissions | greenhouse gases | hydrology | water cycle

Anthropogenic perturbation of the atmospheric water cycle is expressed over a wide range of spatial and temporal scales. Recent global changes resulting from warming-associated increases in saturation vapor pressure have been observed in satellite and reanalysis data (1, 2). Regional impacts related to large-scale land use change are detectible in precipitation data and models (3–5). Humidity anomalies (both positive and negative) have been observed in many urban centers and associated with changes in land cover, direct anthropogenic sources, and interaction of evapotranspiration and condensation processes with the urban heat island effect (6–10).

Fossil fuel combustion releases water vapor to the atmosphere. Assuming an average molar ratio of H_2O to CO_2 emission of 1.5 (see *Water of Combustion*) and current anthropogenic carbon emission rates of 9.5 Pg C/y (11), global combustion vapor emissions total ∼21 Pg/y. At the global scale, these numbers are four orders of magnitude smaller than the gross global exchange of water vapor between the Earth surface and the atmosphere, which totals more than 480,000 Pg/y (12). However, anthropogenic emissions are highly concentrated in space and time and, locally, may be a significant source of vapor and impact atmospheric water cycling, ambient humidity, and photochemistry. Water of combustion has been hypothesized to be an important contributor of urban boundary layer vapor in some studies of urban–rural humidity gradients (13, 14), but in other cases has been dismissed as a minor source (6). Thus far it has not been possible to directly observe or quantify the concentration of combustion-derived vapor in the atmosphere.

Here we report data and modeling that indicates that water of combustion can be identified in the atmospheric boundary layer using stable isotope ratio measurements of ambient water vapor. Our data document winter season boundary layer vapor in Salt Lake City, Utah (SLC; 40.7662°N, 111.8477°W, elevation 1440 m). Salt Lake City is situated in a north–south oriented basin, surrounded on three sides by substantial mountain ranges, and is subject to prolonged cold air inversion events during the winter season. Previous work has documented the accumulation of combustion-derived CO_2 in the boundary layer during these events (15–17). We show that water vapor deuterium excess ($d = \delta^2H - 8 \times \delta^{18}O$) closely tracks changes in CO_2 through inversion events and across a daily cycle dominated by patterns of human activity. Deuterium excess reflects deviations in the coupled H and O isotopic compositions of water from a covariant trend established by equilibrium phase-change reactions in the atmosphere, and has previously been used to diagnose vapor source region conditions, nonequilibrium processes, and vertical mixing (18–21). We demonstrate that combustion-derived water vapor is characterized by a distinctive d value due to its unique mode of production, illustrate that this strong signal is detectible and can be used to quantify the concentration of combustion-derived vapor in the SLC wintertime atmosphere, and demonstrate congruence between these estimates and those derived from a mass-balance model forced by meteorological and emissions data.

Significance

Human activities affect the water cycle in many ways, some of which remain difficult to measure. One such process is emission of water vapor through combustion of fossil fuels, which may be a significant part of the atmospheric water budget in urban centers. It has not previously been possible to uniquely identify combustion-derived water vapor with atmospheric measurements. We introduce a method for the measurement of combustion-derived vapor, and show that this source contributes as much as 13% of surface-level vapor in the atmosphere of one city. The new approach may help researchers monitor sources of greenhouse gas emissions from cities and study the impact of water of combustion on urban weather, quality of life, and atmospheric chemistry.

Author contributions: G.J.B. designed research; G.G., C.S., and G.J.B. performed research; G.G., C.S., S.P.G., R.B., and J.R.E. contributed new reagents/analytic tools; G.G., C.S., and G.J.B. analyzed data; and G.G., C.S., S.P.G., R.B., J.R.E., and G.J.B. wrote the paper.

The authors declare no conflict of interest.

This article is a PNAS Direct Submission.

Freely available online through the PNAS open access option.

[1]To whom correspondence should be addressed. Email: gabe.bowen@utah.edu.

This article contains supporting information online at www.pnas.org/lookup/suppl/doi:10.1073/pnas.1424728112/-/DCSupplemental.

Water Vapor Isotope Record

We measured concentrations of CO_2 and H_2O and the isotope ratios of boundary layer vapor in SLC from December 3, 2013 through January 31, 2014 and report the measurements averaged at 5-min intervals. After allowing for interruptions to instrument operations and quality control screening of the data (*SI Materials and Methods*), our record completeness is 79.5% for water vapor isotope ratios and 98.2% for CO_2 concentration. Vapor δ^2H and $\delta^{18}O$ values during the monitoring period averaged −209.8 parts per thousand (‰) and −26.9‰, respectively, and exhibited a range of short-term and long-term trends and variability (*SI Materials and Methods*). The H and O isotope ratio data are correlated with both ambient surface air temperature ($r^2 = 0.45$ and 0.38 for δ^2H and $\delta^{18}O$, respectively) and the logarithm of specific humidity ($r^2 = 0.20$ and 0.22; all correlations presented in this section are significant at $P < 0.001$ with $n = 12{,}608$). This pattern is consistent with that expected if variation in the distillation of heavy isotopes from air masses within the large-scale circulation was a dominant control on SLC vapor δ^2H and $\delta^{18}O$ values (22–24).

In contrast, values of vapor *d* exhibit distinct patterns of temporal variation (Fig. 1) and much weaker correlation with temperature and humidity ($r^2 = 0.09$ and 0.06, respectively) throughout the duration of the record. Vapor *d* averaged +5.5‰, with particularly high values occurring in early December during the driest multiday interval of the study period. The highest *d* values occurred following a rain event on December 7, and likely reflect moistening of the dry boundary layer by evaporation from raindrops (*SI Materials and Methods*) (24). After mid-December, *d* fluctuated between high values of approximately +10‰, which are typical for boundary layer vapor sampled at many sites worldwide, and values as low as −17.2‰, which are very uncommon in previous vapor isotope studies (18).

The observed *d* values are inversely correlated with concentrations of CO_2 in the SLC boundary layer across the period of record ($r^2 = 0.33$). This correlation is accentuated if we consider data from before and during the first inversion separately from the rest of the record ($r^2 = 0.57$ for December 3–19, 2013; $r^2 = 0.64$ for December 19, 2013 through January 31, 2014). Values of *d* show particularly strong association with CO_2 concentrations through four periods of atmospheric inversion (Fig. 1). At the onset of each inversion, *d* values decline in parallel with increasing CO_2 concentrations, dropping by as much as 25‰ relative to preinversion values over periods of several days of atmospheric stability. Within three of the four inversion periods (periods i, ii, and iv in Fig. 1), *d* values also closely track transient plateaus and reductions in CO_2 concentrations, presumably associated with partial destabilization of the stagnant boundary layer and enhanced vertical or lateral mixing with the free atmosphere.

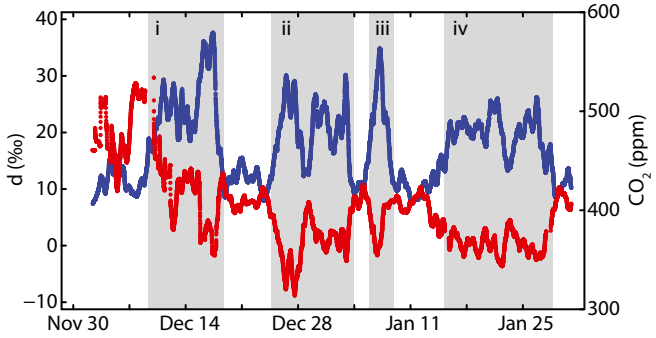

Fig. 1. Observed water vapor D excess (*d*; red curve) and CO_2 concentration (blue) in the SLC urban boundary layer. Data are smoothed using a 12-h moving average. Gray-shaded time periods labeled i–iv indicate four major atmospheric inversion periods.

During a fourth, short-lived inversion (period iii) water vapor *d* values track the growth of boundary layer CO_2 to its peak and then recover rapidly as CO_2 concentrations begin a slower decline. The interval of *d* recovery is characterized by a near tripling of boundary layer specific humidity (*SI Materials and Methods*), suggesting that the decoupling of CO_2 and *d* patterns at this time may reflect the dilution of the boundary layer vapor by mixing with a particularly moist free atmosphere.

Boundary layer *d* and CO_2 are also closely correlated over diurnal timescales, both within and outside of periods of inversion (Fig. 2). The diurnal cycle is dominated by a peak in CO_2 and trough in *d* in the midmorning and a broader CO_2 maximum and *d* minimum from the evening through early morning hours. The morning peak/trough is centered on *ca.* 1000 h local time, with the strongest growth in CO_2 and decline in *d* occurring between 700 h and 1000 h. From *ca.* 1030 h, values begin to recover, reaching "background" values between 1500 h and 1600 h. The nighttime feature, which is exaggerated in magnitude during inversion periods, reaches its zenith at *ca.* 2000 h. Values remain stable until *ca.* 2400 h, when they begin a partial recovery toward the baseline over the following 2–3 h.

The diurnal pattern in CO_2 concentrations has previously been attributed to variations in human emissions and atmospheric conditions throughout the day, including automobile exhaust associated with morning and evening rush hour commuting, nighttime home heating, and dilution of CO_2 during midday boundary layer growth (15). The strong association of vapor *d* with concentrations of emissions-derived CO_2, over both diurnal and multiday timescales, suggests that *d* is likely recording changes in the SLC boundary layer water budget associated with anthropogenic emissions.

Water of Combustion

Given these observations, we hypothesize that the accumulation of combustion-derived water vapor in the SLC urban boundary layer is recorded in the vapor *d* data. To our knowledge the δ^2H and $\delta^{18}O$ values of combustion-derived H_2O have not previously been assessed. We estimate these values, considering two sources: (*i*) combustion of natural gas for home heating and (*ii*) combustion of gasoline for transportation.

Natural gas combusts according to

$$CH_4 + 2O_2 \rightarrow 2H_2O + CO_2. \quad [1]$$

The sole H source in this reaction is H from the methane molecule, which for biogenic methane ranges from *ca.* −280‰ to −180‰, depending on the δ^2H of formation water (25). Assuming negligible loss of hydrogen to combustion byproducts, H_2O is the only hydrogen-containing product, and we therefore assume that the water H is unfractionated relative to the CH_4 source. The other reactant and sole source of oxygen, atmospheric O_2, has a uniform $\delta^{18}O \approx 23.9‰$ (26). Assuming ideal combustion, the reactant oxygen is partitioned among H_2O and CO_2 according to

$$f_{H2O} = ef/(ef + 2), \quad [2]$$

where f_{H2O} is the fraction of the oxygen reactant accumulating in the H_2O product ($1 - f_{H2O} = f_{CO2}$) and the emission factor *ef* is the ratio of the stoichiometric coefficients for H_2O and CO_2 in the balanced reaction (*ef* = 2 for Eq. **1**). Under equilibrium conditions at 100 °C, CO_2 is enriched in ^{18}O by *ca.* 29‰ relative to CO_2 (27). The extent of isotopic equilibration between these species within fossil fuel combustion systems is unknown and likely variable (28), so here we evaluate a range of conditions from no equilibration ($\delta^{18}O_{H2O} = \delta^{18}O_{CO2} = +23.9‰$) to complete equilibration ($\delta^{18}O_{H2O} = \delta^{18}O_{CO2} - 29$). For this latter case, the $\delta^{18}O_{H2O}$ from combustion is

$$\delta^{18}O_{H2O} = \delta^{18}O_{atm} - 29 \times f_{CO2}. \quad [3]$$

These endmember scenarios yield 9.4‰ < $\delta^{18}O_{H2O}$ < 23.9‰ and −471‰ < d < −255‰ for CH_4-derived H_2O.

The other major source of combustion-derived water vapor is the combustion of gasoline for transportation. Gasoline δ^2H can vary widely depending on geological and environmental processes surrounding the formation of the crude oil, as well as some postdepositional processes (29). In addition, mixing of crude oil from different sources is common at refineries (30), which further obfuscates direct connections between crude oil δ^2H values and δ^2H values of automobile gasoline. We approximate δ^2H values for SLC gasoline based on measurements of crude oils from terrestrial basins, such as those of the high-producing Green River Formation in northeastern Utah, southwestern Wyoming, and western Colorado, adopting a range of −250‰ < δ^2H < −140‰ (31).

Although gasoline consists of a mixture of alkanes (C_4 through C_{10}) as well as other minor additives, we here approximate its composition as that of 2,2,4-trimethylpentane (C_8H_{18}, an isomer of octane), a primary constituent of gasoline. The 2,2,4-trimethylpentane combusts according to the following equation:

$$2C_8H_{18} + 25O_2 \rightarrow 18H_2O + 16CO_2. \quad [4]$$

Using the formulation described above, with ef = 1.125 for C_8H_{18}, we estimate values of 5.3‰ < $\delta^{18}O_{H2O}$ < 23.9‰ and −441‰ < d < −183‰ for the combustion of gasoline. We validated these estimates by measuring isotope ratios of water cryogenically trapped from the tailpipes of two automobiles, which are consistent with the predicted range of gasoline-derived vapor isotope values and suggest partial to complete oxygen isotope equilibration between CO_2 and H_2O in the emissions from these vehicles (Fig. 3). Previously published data on the $\delta^{18}O$ values of CO_2 from gasoline engine combustion also suggest substantial isotopic equilibration and are consistent with our data (28).

This analysis suggests that the low d values measured for SLC boundary layer vapor during periods of inversion and during morning and overnight periods of CO_2 accumulation can be explained by the addition of combustion-derived water vapor to a background pool of vapor inherited from the free troposphere. Almost all inversion period vapor values are intermediate between observed, preinversion background vapor values and the measured and estimated combustion vapor values (Fig. 3 and *SI Materials and Methods*). Using the measured automobile exhaust vapor to define a hypothetical isotopic endmember for water of combustion, we estimate that combustion-derived vapor comprised as much as 13% of the total boundary layer moisture during inversion periods.

Despite the strong evidence for a combustion-derived source of low-d vapor to the SLC boundary layer, we considered a range of other water vapor sources that might influence the isotopic composition of atmospheric vapor during inversions. Vapor derived from most surface water—e.g., evaporation of snow melt water or sublimation from snow—is unlikely to be a major source to the atmosphere during cold air inversions. Moreover, this water has high d values (>+10‰) due to kinetic fractionation during evaporation (24, 32) and thus cannot explain the anomalously low d values of boundary layer vapor. Vapor evaporated from the Great Salt Lake (GSL, *ca.* 30 km from sampling location) may be a more significant source given that lake water temperatures are warmer than those of the atmosphere throughout the winter, and this vapor is also expected to have a distinctive isotopic composition due to the high degree of evapoconcentration characterizing the lake water. We use observed GSL water isotope ratios (33) and a model for isotope fractionation during evaporation (32), modified to account for the high lake water salinity (24, 34), to estimate the range of δ^2H and $\delta^{18}O$ values expected for lake-derived vapor (see *SI Materials and Methods*). Although the estimates include d values < 10‰, the distribution of δ^2H and $\delta^{18}O$ values for this source cannot account for the observed boundary layer vapor values through mixing with background atmospheric vapor (Fig. 3).

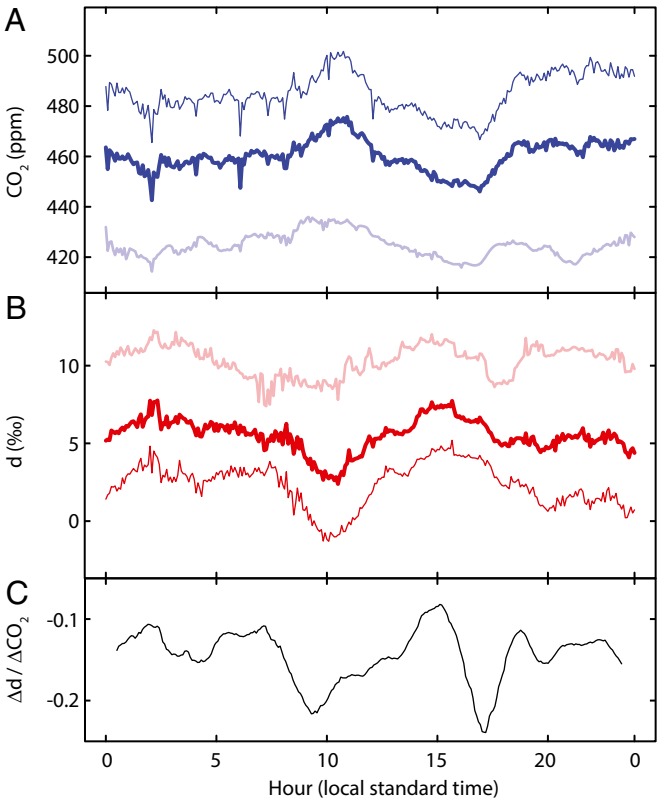

Fig. 2. Average diurnal cycles of CO_2 concentrations (*A*) and water vapor d values (*B*) in the SLC urban boundary layer. Data are averaged for inversion periods (thin line), noninversion periods (faint line), and the entire record (bold line). Values in *C* show the ratio of the d change relative to that for CO_2, calculated relative to the maximum (d) or minimum (CO_2) values [(d − d_{max})/(CO_2 − CO_{2min})], for the inversion period data. Data in *C* are smoothed with a 1-h moving average.

In addition to the variation among fuels described by ef, the ratio of H_2O to CO_2 emission from different combustion sources will vary due to differing degrees of condensation in exhaust systems. In particular, current generation high-efficiency natural gas furnaces use condensers to extract heat from exhaust vapor, and are expected to have particularly low H_2O/CO_2 emission ratios. This condensation, which takes place in a water-saturated environment, likely involves isotopic equilibrium: Although it may shift the exhaust vapor δ^2H and $\delta^{18}O$, we expect it to have little effect on the vapor d values. Because of the drastically different H_2O/CO_2 emission ratios associated with different combustion sources, however, paired urban boundary layer measurements of CO_2 and estimates of combustion-derived vapor from d may be useful for diagnosing emission sources in the urban environment. The diurnal cycles observed here provide a qualitative indication of the existence of such a signal, in that the ratio of d change to CO_2 change during the overnight home-heating period is about half of that observed in association with the morning and evening commuting periods (Fig. 2*C*). Although this could indicate a higher d value for nighttime combustion sources, our estimates suggest that CH_4-derived should actually have a lower d than gasoline-derived vehicle exhaust, and the alterative explanation is a substantial reduction in the mean ratio

of H_2O to CO_2 emissions during the night. Quantitative adoption of this approach will be challenging and require a more thorough understanding of controls on d for water emitted from different combustion processes (including O-bearing fuels) as well as accounting for other sources and sinks for boundary layer vapor or the use of independent tracers to help separate combustion and noncombustion influences on d values. One such tracer may be ^{17}O (28, 35), which, through recent advances in laser spectroscopy, is now a potential candidate for inclusion in atmospheric monitoring (36, 37). With such information, d may prove to be a useful complement to other tracers used in partitioning urban emissions, such as $\delta^{13}CO_2$ and [CO] (17, 38).

Modeling

We compare our results with a bottom-up simulation of atmospheric water balance driven by meteorological data and gridded emissions data (Fig. 4). As detailed in the *SI Materials and Methods*, the CO_2 multiple box model of ref. 15 was adapted to also represent boundary layer water vapor from combustion (q_c) on a 10 km × 10 km grid over Salt Lake Valley. CO_2 and H_2O emissions were prescribed based on the Vulcan emissions inventory (39). As previously demonstrated (15), the model was able to simulate realistic variations in boundary layer CO_2 concentrations throughout the monitoring period (r^2 = 0.42; Fig. 4*A*). Values of q_c generated by the model were converted to d using

$$d = (d_c q_c + d_a q_a)\, q^{-1}, \qquad [5]$$

where $d_c = -225‰$ was prescribed based on Fig. 3, the background water vapor concentration $q_a = q - q_c$, and d_a was a smooth function representing the deuterium excess of vapor in the free troposphere (Fig. 4*B*). Although the model failed to predict the extreme low d values observed on some inversion days, it captured the majority of the observed pattern of variation in d throughout the period of observation (r^2= 0.59).

Both the model and the observed data can be used to derive continuous estimates of the fraction (χ) of boundary layer vapor derived from combustion. Using a common estimate of d_a values and Eq. **5**, the two independent estimates of χ show encouraging convergence (Fig. 4*C*). Maximum combustion-derived vapor concentrations reach *ca.* 200 ppm during inversion periods in mid-December and in late December through early January. Given observed boundary layer humidity values during these events, this translates to a 5–10% total contribution of combustion-derived vapor, consistent with the rough estimates from the simple two-endmember mixing calculation in *Water of Combustion*. The estimates presented in Fig. 4*C* assume a continuous evolution of d_a values as represented by the optimized smooth function. Thus, they may underestimate the cumulative contribution of combustion-derived vapor to boundary layer moistening during inversions events if the d values of the free troposphere evolve more discretely than represented by the function, i.e., in response to the passage of synoptic systems (18).

The modeled diurnal cycle shows an earlier initiation of the morning d increase and a broader afternoon peak than seen in the data (Fig. 5*A*) but captures the amplitude and the overall structure with sufficient fidelity to provide insights into the forcing driving variation in q_c. The modeled diurnal cycle of d is, to first order, a scaling of the diurnal cycle of χ because differentiating (5) yields

$$\frac{\partial d}{\partial t} = \frac{\partial \chi}{\partial t}(d_c - d_a) + \frac{\partial d_a}{\partial t}(1 - \chi), \qquad [6]$$

where the mean absolute value of the first term is an order of magnitude larger than the second, providing further support for

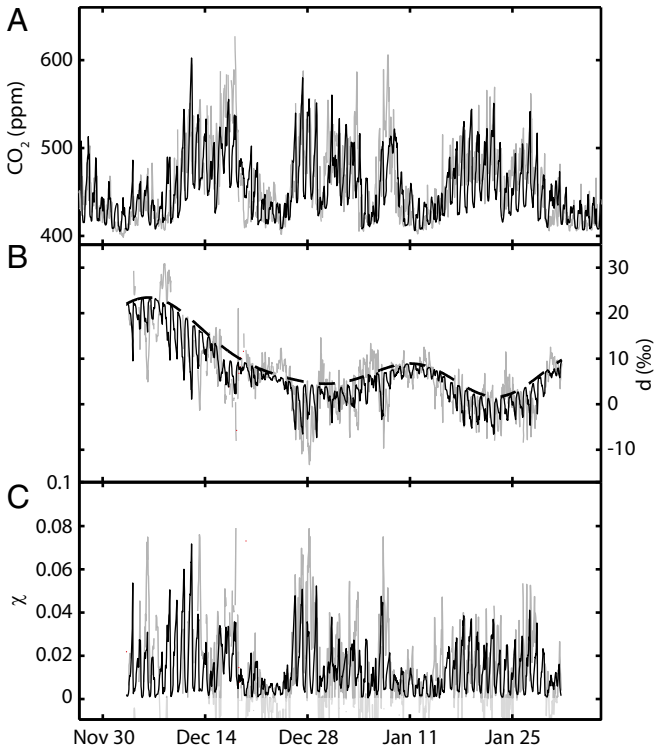

Fig. 4. Modeled (black) and observed (gray) atmospheric tracer properties throughout the study interval. Direct measurements of CO_2 concentration (*A*) and d (*B*) are compared with results from an atmospheric mass balance model forced by meteorological and emissions data. In *B*, the dashed line shows the function used to represent the d values of vapor in the free troposphere (d_a), and the d value of combustion-derived vapor (d_c) was prescribed as −225‰. For d_a, a parsimonious form was specified using harmonics 0 through 4 plus a trend term, and its parameters were optimized based on the residual sum of squared errors in d. In *C*, model estimates of the fraction (χ) of specific humidity derived from combustion are compared with equivalent estimates calculated directly from the observed d data (compare Fig. 3). Both estimates use the d_a curve from panel *B*. Light gray values are times where $d > d_a$, implying nonphysical negative χ.

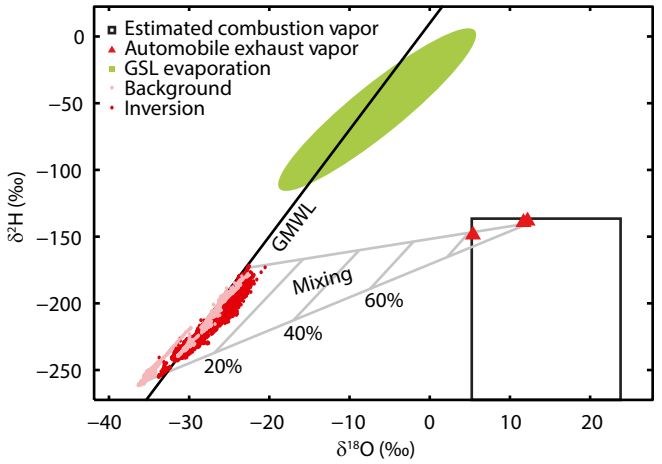

Fig. 3. Boundary layer water vapor isotope data for inversion (red) and preinversion background (light red) conditions, with measured and estimate values for potential vapor sources. Mixing envelope shows approximate range of values and associated percent contribution of combustion-derived vapor for linear mixtures between background vapor and the highest δ^2H and $\delta^{18}O$ values measured for exhaust vapor. The approximate range of GSL evaporation values was calculated using a model of evaporative fractionation, as described in *SI Materials and Methods*. GMWL, global meteoric water line.

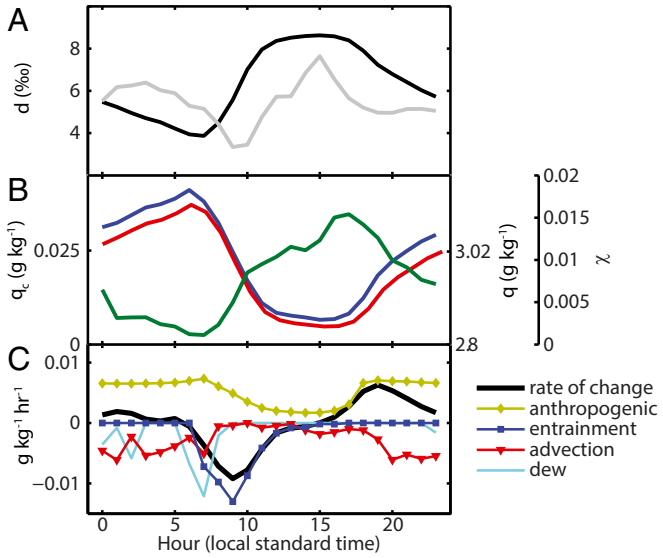

Fig. 5. Box model analysis of the diurnal cycle of d. (*A*) Comparison of observed (gray) and modeled (black) mean diurnal cycle of d across the entire study period. (*B*) Diurnal cycle of modeled specific humidity from combustion (q_c, blue curve), observed total specific humidity (q, green), and the fraction (χ) of q consisting of combustion-derived vapor (red). (*C*) The modeled rate of change of q_c is decomposed into component terms (see legend): The anthropogenic term is upward water vapor flux from combustion at the surface, the entrainment term accounts for air drawn in from above during daytime mixed layer growth, the advection term represents transport by wind, and the dew term indicates losses to the surface by dewfall or frost (dew values shown as medians rather than means because of their strong negative skewness).

the interpretation of variation in the record of d in terms of the accumulation of combustion-derived vapor. The diurnal cycles of q and q_c are strongly negatively correlated, yielding a diurnal cycle of χ closely resembling the structure of q_c (Fig. 5*B*). Decomposing the component forcing on q_c in the model (Fig. 5*C*) shows that q_c increases overnight because the upward flux of water vapor from combustion exceeds removal by wind, but this increase slows before sunrise because of losses to dewfall or frost. During the day, q_c decreases because mixed layer growth entrains lower-q_c air from above, and the associated weakening of horizontal gradients lessens the importance of removal by wind. Sunset brings the cycle back to the overnight period where anthropogenic flux exceeds removal by wind, especially shortly after sunset, when horizontal gradients are still weak from daytime mixing (around 1900 h).

Conclusions

We have demonstrated that traditional light stable isotope measurements of atmospheric water vapor record information on the concentration of combustion-derived water vapor, that these concentrations can be significant in the urban boundary layer, and that they vary over a range of timescales in response to changes in source strength and atmospheric mixing. These findings have implications that span a range of fields. Recognition of the extreme, negative d values associated with water of combustion is important for the growing number of water vapor isotope studies focusing on other aspects of the atmospheric water budget, and has implications for instrument siting and data interpretation in monitoring efforts such as the National Ecological Observatory Network, which will make continuous water vapor isotope ratio measurements at tens of sites across the United States (40). It is possible that previous records of water vapor d from other sites record signals related to combustion-derived vapor; such effects are not immediately apparent in a recent metaanalysis of vapor d records (18) but a more thorough evaluation of the data may be warranted. As discussed in *Water of Combustion*, there is potential for the application of boundary layer d measurements to be used in conjunction with other tracers in efforts to partition urban emission sources of greenhouse gases and other pollutants. Lastly, the water isotope signature of combustion offers new opportunities to investigate the role of combustion as an integrated component of the urban hydrological cycle. Our data suggest that combustion is a nontrivial part of this cycle under some conditions. Combustion water emissions contribute significantly to the growth of boundary layer humidity through atmospheric inversions in SLC, and, as such, likely impact the local meteorology, atmospheric chemistry, and human comfort during these events. Understanding and effectively managing the water cycle of urban areas represents a key challenge for sustainability science, and our work suggests that water of combustion is an important and perhaps underappreciated component of this cycle.

Materials and Methods

Water vapor isotope ratios were measured from an intake ~4 m above the roof of the eight-story William Browning Building on the campus of the University of Utah using a Picarro L2130-i cavity ring-down spectrometer. Vapor isotopologue measurements were corrected for concentration dependence of the analyzer and were calibrated to the Vienna Standard Mean Ocean Water/Standard Light Antarctic Precipitation reference scale based on measurements of two laboratory reference waters made approximately daily throughout the period of study. Raw ~1-Hz measurements were averaged to obtain 5-min means and screened for quality control. Measurement precision of d values in the processed dataset is estimated to be 2.3‰ (1 σ; see *SI Materials and Methods*).

The isotopic data were merged with weather data from a colocated weather station (mesowest.utah.edu, University of Utah William Browning Building Station) and independent CO_2 monitoring data before analysis. CO_2 measurements were made at the Aline Wilmot Skaggs Biology Building, ~500 m from the water vapor measurement site, using a Li-Cor Li-7000 infrared gas analyzer. Measured values were calibrated against analyses of gas from four reference cylinders and screened using standard quality control criteria.

Water vapor was collected from the exhaust pipe of two vehicles, a 1991 Toyota Land Cruiser and a 2006 Mercury Milan, by cryogenic trapping. Frozen vapor was thawed and the resulting liquid analyzed using a Picarro L2130-i cavity ring-down spectrometer. Instrument operation and data reduction procedures are described in ref. 41.

The multiple box model used to simulate the water balance and isotopic composition of the Salt Lake Valley boundary layer was modified from previous work by ref. 15. The model tracked fluxes of water vapor into, out of, and within a grid of 10 km^2 variable-depth boxes representing the boundary layer. Lateral and upper boundary conditions were specified using station observations and reanalysis data for the period of study (see *SI Materials and Methods*). Surface (combustion) emissions were specified by rescaling CO_2 emissions reported in the "Vulcan" gridded emissions product (39) (see *SI Materials and Methods*).

ACKNOWLEDGMENTS. Financial support was provided by U.S. National Science Foundation Grants EF-01241286 and EF-01240142 and by Department of Energy Grant DE-SC-001-0624. C.S. was supported by NOAA Climate Program Office's Atmospheric Chemistry, Carbon Cycle, and Climate Program, Grant NA14OAR4310178. This work was made possible by resources and support from the University of Utah Center for High Performance Computing.

1. Chung E-S, Soden B, Sohn BJ, Shi L (2014) Upper-tropospheric moistening in response to anthropogenic warming. *Proc Natl Acad Sci USA* 111(32):11636–11641.
2. Trenberth KE, Fasullo J, Smith L (2005) Trends and variability in column-integrated atmospheric water vapor. *Clim Dyn* 24(7-8):741–758.
3. Lo M-H, Famiglietti JS (2013) Irrigation in California's Central Valley strengthens the southwestern U. S. water cycle. *Geophys Res Lett* 40(2):301–306.
4. DeAngelis A, et al. (2010) Evidence of enhanced precipitation due to irrigation over the Great Plains of the United States. *J Geophys Res* 115(D15):D15115.
5. Gordon LJ, et al. (2005) Human modification of global water vapor flows from the land surface. *Proc Natl Acad Sci USA* 102(21):7612–7617.
6. Holmer B, Eliasson I (1999) Urban–rural vapour pressure differences and their role in the development of urban heat islands. *Int J Climatol* 19(9):989–1009.

7. Tapper NJ (1990) Urban influences on boundary layer temperature and humidity: Results from Christchurch, New Zealand. *Atmos Environ, Part B* 24(1):19–27.
8. Grimmond CSB, Oke TR (1999) Rates of evaporation in urban areas. Impacts of urban growth on surface and ground waters. *IAHS Publ* 259:235–243.
9. Richards K (2005) Urban and rural dewfall, surface moisture, and associated canopy-level air temperature and humidity measurements for Vancouver, Canada. *Boundary-Layer Meteorol* 114(1):143–163.
10. Fortuniak K, Kłysik K, Wibig J (2006) Urban–rural contrasts of meteorological parameters in Łódź. *Theor Appl Climatol* 84(1-3):91–101.
11. Ciais P, et al. (2013) Carbon and other biogeochemical cycles. *Climate Change 2013: The Physical Science Basis. Contribution of Working Group I to the Fifth Assessment Report of the Intergovernmental Panel on Climate Change*, eds Stocker TF, et al. (Cambridge Univ Press, Cambridge, UK), pp 465–570.
12. Trenberth KE, Smith L, Qian T, Dai A, Fasullo J (2007) Estimates of the global water budget and its annual cycle using observational and model data. *J Hydrometeorol* 8(4):758–769.
13. Ackerman B (1987) Climatology of Chicago area urban-rural differences in humidity. *J Clim Appl Meteorol* 26(3):427–430.
14. Hage KD (1975) Urban-rural humidity differences. *J Appl Meteorol* 14:1277–1283.
15. Strong C, Stwertka C, Bowling DR, Stephens BB, Ehleringer JR (2011) Urban carbon dioxide cycles within the Salt Lake Valley: A multiple-box model validated by observations. *J Geophys Res* 116(D15):D15307.
16. Pataki DE, Bowling DR, Ehleringer JR, Zobitz JM (2006) High resolution atmospheric monitoring of urban carbon dioxide sources. *Geophys Res Lett* 33(3):L03813.
17. Pataki DE, Bowling DR, Ehleringer JR (2003) Seasonal cycle of carbon dioxide and its isotopic composition in an urban atmosphere: Anthropogenic and biogenic effects. *J Geophys Res* 108(D23):4735.
18. Welp LR, et al. (2012) A meta-analysis of water vapor deuterium-excess in the mid-latitude atmospheric surface layer. *Global Biogeochem Cycles* 26(3):GB3021.
19. Bowen GJ, Kennedy CD, Henne PD, Zhang T (2012) Footprint of recycled water subsidies downwind of Lake Michigan. *Ecosphere* 3(6):53.
20. Benetti M, et al. (2014) Deuterium excess in marine water vapor: Dependency on relative humidity and surface wind speed during evaporation. *J Geophys Res* 119(2): 584–593.
21. Aemisegger F, et al. (2014) Deuterium excess as a proxy for continental moisture recycling and plant transpiration. *Atmos Chem Phys* 14(8):4029–4054.
22. Worden J, Noone D, Bowman K; Tropospheric Emission Spectrometer Science Team and Data contributors (2007) Importance of rain evaporation and continental convection in the tropical water cycle. *Nature* 445(7127):528–532.
23. Rozanski K, Araguas-Araguas L, Gonfiantini R (1993) Isotopic patterns in modern global precipitation. *Climate Change in Continental Isotopic Records*, eds Swart PK, Lohmann KC, McKenzie J, Savin S, Geophysical Monograph Series (Am Geophys Union, Washington, DC), Vol 78, pp 1–36.
24. Gat JR (1996) Oxygen and hydrogen isotopes in the hydrologic cycle. *Annu Rev Earth Planet Sci* 24:225–262.
25. Whiticar MJ (1999) Carbon and hydrogen isotope systematics of bacterial formation and oxidation of methane. *Chem Geol* 161(1):291–314.
26. Barkan E, Luz B (2005) High precision measurements of $^{17}O/^{16}O$ and $^{18}O/^{16}O$ ratios in H_2O. *Rapid Commun Mass Spectrom* 19(24):3737–3742.
27. Friedman I, O'Neil JR (1977) Compilation of stable isotope fractionation factors of geochemical interest. *U.S. Geol Surv Prof Pap* 440-KK:1–12.
28. Horváth B, Hofmann MEG, Pack A (2012) On the triple oxygen isotope composition of carbon dioxide from some combustion processes. *Geochim Cosmochim Acta* 95(0): 160–168.
29. Li M, et al. (2001) Hydrogen isotopic compositions of individual alkanes as a new approach to petroleum correlation: Case studies from the Western Canada Sedimentary Basin. *Org Geochem* 32(12):1387–1399.
30. Bush S, Pataki D, Ehleringer J (2007) Sources of variation in $\delta^{13}C$ of fossil fuel emissions in Salt Lake City, USA. *Appl Geochem* 22(4):715–723.
31. Xiong Y, Geng A, Pan C, Liu D, Peng P (2005) Characterization of the hydrogen isotopic composition of individual *n*-alkanes in terrestrial source rocks. *Appl Geochem* 20(3):455–464.
32. Craig H, Gordon LI (1965) Deuterium and oxygen-18 variations in the ocean and the marine atmosphere. *Proceedings of a Conference on Stable Isotopes in Oceanographic Studies and Paleotemperatures*, ed Tongiorgi E (V. Lishi, Pisa, Italy), pp 9–130.
33. Nielson KE, Bowen GJ (2010) Hydrogen and oxygen in brine shrimp chitin reflect environmental water and dietary isotopic composition. *Geochim Cosmochim Acta* 74(6):1812–1822.
34. Horita J, Rozanski K, Cohen S (2008) Isotope effects in the evaporation of water: A status report of the Craig-Gordon model. *Isotopes Environ Health Stud* 44(1):23–49.
35. Uemura R, Barkan E, Abe O, Luz B (2010) Triple isotope composition of oxygen in atmospheric water vapor. *Geophys Res Lett* 37(4):L04402.
36. Steig E, et al. (2013) Calibrated high-precision ^{17}O-excess measurements using laser-current tuned cavity ring-down spectroscopy. *Atmos Meas Tech* 7:2421–2435.
37. Berman ES, Levin NE, Landais A, Li S, Owano T (2013) Measurement of δ18O, δ17O, and 17O-excess in water by off-axis integrated cavity output spectroscopy and isotope ratio mass spectrometry. *Anal Chem* 85(21):10392–10398.
38. Brioude J, et al. (2011) Top-down estimate of anthropogenic emission inventories and their interannual variability in Houston using a mesoscale inverse modeling technique. *J Geophys Res* 116(D20):D20305.
39. Gurney KR, et al. (2009) High resolution fossil fuel combustion CO_2 emission fluxes for the United States. *Environ Sci Technol* 43(14):5535–5541.
40. Kao RH, et al. (2012) NEON terrestrial field observations: Designing continental-scale, standardized sampling. *Ecosphere* 3(12):art115.
41. Good SP, Mallia DV, Lin JC, Bowen GJ (2014) Stable isotope analysis of precipitation samples obtained via crowdsourcing reveals the spatiotemporal evolution of Superstorm Sandy. *PLoS ONE* 9(3):e91117.